
Learning Multimodal VAEs through Mutual Supervision

Tom Joy*
University of Oxford

Yuge Shi
University of Oxford

Philip H.S. Torr
University of Oxford

Tom Rainforth
University of Oxford

Sebastian M. Schmon
Improbable

N. Siddharth
University of Edinburgh

Abstract

Multimodal variational autoencoders (VAEs) seek to model the joint distribution over heterogeneous data (e.g. vision, language), whilst also capturing a shared representation across such modalities. Prior work has typically combined information from the modalities by reconciling idiosyncratic representations directly in the recognition model through explicit products, mixtures, or other such factorisations. Here we introduce a novel alternative, the **M**utually **s**up**E**rvised **M**ultimodal VAE (MEME), that avoids such explicit combinations by repurposing semi-supervised VAEs to combine information between modalities *implicitly* through mutual supervision. This formulation naturally allows learning from partially-observed data where some modalities can be entirely missing—something that most existing approaches either cannot handle, or do so to a limited extent. We demonstrate that MEME outperforms baselines on standard metrics across *both* partial and complete observation schemes on the MNIST-SVHN (image–image) and CUB (image–text) datasets. We also contrast the quality of the representations learnt by mutual supervision against standard approaches and observe interesting trends in its ability to capture relatedness between data.

1 Introduction

Modelling the generative process underlying heterogenous data, particularly data spanning multiple perceptual modalities such as vision or language, can be enormously challenging. Consider for example, the case where data spans across photographs and sketches of objects. Here, a data point, comprising of an instance from each modality, is constrained by the fact that the instances are related and must depict the *same* underlying abstract concept. An effective model not only needs to faithfully generate data in each of the different modalities, it also needs to do so in a manner that preserves the underlying relation between modalities. Learning a model over multimodal data thus relies on the ability to bring together information from quite idiosyncratic sources in such a way as to overlap on aspects they relate on, while remaining disjoint otherwise.

Variational autoencoders (VAEs) (Kingma and Welling, 2014) are a class of deep generative models that are particularly well-suited for multimodal data as they employ the use of *encoders*—learnable mappings from high-dimensional data to lower-dimensional representations—that provide the means to combine information across modalities. They can also be adapted to work on data with instances missing for some modalities; a consequence of the difficulties inherent in obtaining and curating heterogenous data. Much of the work in multimodal VAEs involves exploring different ways to model and formalise the combination of information with a view to improving the quality of the learnt models (see § 2).

*Contact tomjoy@robots.ox.ac.uk

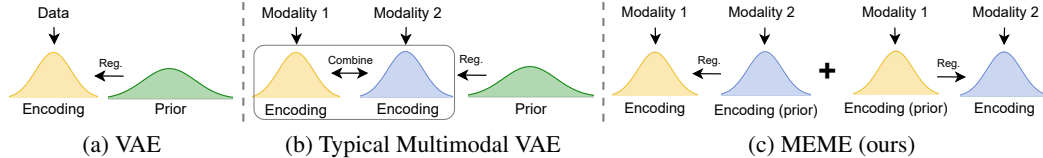


Figure 1: Constraints on the representations. **(a) VAE**: A prior regularises the data encoding distribution through KL. **(b) Typical multimodal VAE**: Encodings for different modalities are first explicitly combined, with the result regularised by a prior through KL. **(c) MEME (ours)**: Leverage semi-supervised VAEs to cast one modality as a conditional prior, implicitly supervising/regularising the other through the VAE’s KL. Mirroring the arrangement to account for KL asymmetry enables multimodal VAEs through mutual supervision.

Prior approaches typically combine information through *explicit* specification as products (Wu and Goodman, 2018), mixtures (Shi et al., 2019), combinations of such (Sutter et al., 2021), or through additional regularisers on the representations (Sutter et al., 2020; Suzuki et al., 2016). Here, we explore an alternate approach that leverages advances in semi-supervised VAEs (Joy et al., 2021; Siddharth et al., 2017) to repurpose existing regularisation in the VAE framework as an *implicit* means by which information is combined across modalities (see Figure 1).

We develop a novel formulation for multimodal VAEs that views the combination of information through a semi-supervised lens, as *mutual supervision* between modalities. We term this approach **Mutually supERvised Multimodal VAE (MEME)**. Our approach not only avoids the need for additional explicit combinations, but it also naturally extends to *learning* in the partially-observed setting—something that most prior approaches cannot handle. We evaluate MEME on standard metrics for multimodal VAEs across both partial *and* complete data settings, on two typical multimodal data domains: MNIST-SVHN (image-image) and CUB (image-text), and show that it outperforms prior work. We additionally investigate the ability of multimodal VAEs to capture the ‘relatedness’ across modalities in their learnt representations, by comparing and contrasting the characteristics of our implicit approach against prior work.

2 Related work

Prior approaches to multimodal VAEs can be broadly categorised in terms of the explicit combination of representations (distributions) from different modalities, namely concatenation and factorization.

Concatenation: Models in this category learn joint representation by either concatenating the inputs themselves or their modality-specific representations. Examples for the former includes early work in multimodal VAEs such as the JMVAE (Suzuki et al., 2016), triple ELBO (Vedantam et al., 2018) and MFM (Tsai et al., 2019), which define a joint encoder over concatenated multimodal data. Such approaches usually require the training of auxiliary modality-specific components to handle the partially-observed setting, with missing modalities, at test time. They also cannot learn from partially-observed data. In very recent work, Gong et al. (2021) propose VSAE where the latent representation is constructed as the concatenation of modality-specific encoders. Inspired by VAEs that deal with imputing pixels in images such as VAEAC (Ivanov et al., 2019), Partial VAE (Ma et al., 2018), MIWAE (Mattei and Frellsen, 2019), HI-VAE (Nazábal et al., 2020) and pattern-set mixture model (Ghalebikesabi et al., 2021), VSAE can learn in the partially-observed setting by incorporating a modality mask. This, however, introduces additional components such as a collective proposal network and a mask generative network, while ignoring the need for the joint distribution over data to capture some notion of the relatedness between modalities.

Factorization: In order to handle missing data at test time without auxiliary components, recent work propose to factorize the posterior over all modalities as the product (Wu and Goodman, 2018) or mixture (Shi et al., 2019) of modality-specific posteriors (experts). Following this line of work, Sutter et al. (2021) proposes to combine the two approaches (MoPoE-VAE) to improve learning in settings where the number of modalities exceeds two. In contrast to these methods, mmJSD (Sutter et al., 2020) combines information not in the posterior, but in a “dynamic prior”, defined as a function (either mixture or product) over the modality-specific posteriors as well as pre-defined prior.

Table 1 provides a high-level summary of prior work. Note that all the prior approaches have some explicit form of joint representation or distribution, where some of them induces the need for auxiliary components to deal with missing data at test time, while others are established without significant theoretical benefits. By building upon a semi-supervised framework, our method MEME circumvents

this issue to learn representations through mutual supervision between modalities, and is able to deal with missing data at train or test time naturally without additional components.

Table 1: We examine four characteristics: The ability to handle partial observation at test and train time, the form of the joint distribution or representation in the bi-modal case (\mathbf{s} , \mathbf{t} are modalities), and additional components. (✓) indicates a theoretical capability that is not verified empirically.

	Partial Test	Partial Train	Joint repr./dist.	Additional
JMVAE	✓	✗	$q_{\Phi}(\mathbf{z} \mathbf{s}, \mathbf{t})$	$q_{\phi_s}(\mathbf{z} \mathbf{s}), q_{\phi_t}(\mathbf{z} \mathbf{t})$
tELBO	✓	✗	$q_{\Phi}(\mathbf{z} \mathbf{s}, \mathbf{t})$	$q_{\phi_s}(\mathbf{z} \mathbf{s}), q_{\phi_t}(\mathbf{z} \mathbf{t})$
MFM	✓	✗	$q_{\Phi}(\mathbf{z} \mathbf{s}, \mathbf{t})$	$q_{\phi_s}(\mathbf{z} \mathbf{s}), q_{\phi_t}(\mathbf{z} \mathbf{t})$
VSVAE	✓	✓	$\text{concat}(z_s, z_t)$	mask generative network
MVAE	✓	(✓)	$q_{\phi_s}(\mathbf{z} \mathbf{s})q_{\phi_t}(\mathbf{z} \mathbf{t})p(\mathbf{z})$	sub-sampling
MMVAE	✓	✗	$q_{\phi_s}(\mathbf{z} \mathbf{s}) + q_{\phi_t}(\mathbf{z} \mathbf{t})$	-
MoPoE	✓	(✓)	$q_{\phi_s}(\mathbf{z} \mathbf{s}) + q_{\phi_t}(\mathbf{z} \mathbf{t}) + q_{\phi_s}(\mathbf{z} \mathbf{s})q_{\phi_t}(\mathbf{z} \mathbf{t})$	-
mmJSD	✓	✗	$f(q_{\phi_s}(\mathbf{z} \mathbf{s}), q_{\phi_t}(\mathbf{z} \mathbf{t}), p(\mathbf{z}))$	-
Ours	✓	✓	-	-

3 Method

Consider a scenario where we are given a data spanning two modalities, \mathbf{s} and \mathbf{t} . The data is curated in pairs (\mathbf{t}, \mathbf{s}) of these modalities, which might be thought of *pars pro toto* as “style” and “text”, although we are by no means restricted to particular data types. We will further assume that some proportion of observations have one of the modalities missing, leaving us with partially-observed data. Using $\mathcal{D}_{\mathbf{s}, \mathbf{t}}$ to denote the proportion containing fully observed pairs from both modalities, and $\mathcal{D}_{\mathbf{s}}, \mathcal{D}_{\mathbf{t}}$ for the proportion containing observations only from modality \mathbf{s} and \mathbf{t} respectively, we can decompose the data as $\mathcal{D} = \mathcal{D}_{\mathbf{s}} \cup \mathcal{D}_{\mathbf{t}} \cup \mathcal{D}_{\mathbf{s}, \mathbf{t}}$.

In aid of clarity, we will introduce our method by confining attention to this bi-modal case, providing a discussion on generalising beyond two modalities later. Following established notation in the literature on VAEs, we will denote the generative model using p , latent variable using \mathbf{z} , and the encoder, or recognition model, using q . Subscripts for the generative and recognition models, where indicated, denote the parameters of deep neural networks associated with that model.

3.1 Semi-Supervised VAEs

To develop our approach we draw inspiration from semi-supervised VAEs which use additional information, typically data labels, to extend the generative model. This facilitates learning tasks such as disentangling latent representations and performing intervention through conditional generation. In particular, we will build upon the work of Joy et al. (2021), who suggests to supervise latent representations in VAEs with partial label information by forcing the encoder, or recognition model, to channel the flow of information as $\mathbf{s} \rightarrow \mathbf{z} \rightarrow \mathbf{t}$. They demonstrate that the model learns latent representations, \mathbf{z} , of data, \mathbf{s} , that can be faithfully identified with label information \mathbf{t} .

Figure 2 shows a modified version of the graphical model from Joy et al. (2021), extracting just the salient components, and avoiding any other additional constraints therein. The label, here \mathbf{t} , is denoted as partially observed as not all observations \mathbf{s} have associated labels. Note that, following the information flow argument, the generative model factorises as $p_{\theta, \psi}(\mathbf{s}, \mathbf{z}, \mathbf{t}) = p_{\theta}(\mathbf{s} | \mathbf{z}) p_{\psi}(\mathbf{z} | \mathbf{t}) p(\mathbf{t})$ (solid arrows) whereas the recognition model factorises as $q_{\phi, \varphi}(\mathbf{t}, \mathbf{z} | \mathbf{s}) = q_{\varphi}(\mathbf{t} | \mathbf{z}) q_{\phi}(\mathbf{z} | \mathbf{s})$ (dashed arrows). This autoregressive formulation of both the generative and recognition models is what enables the “supervision” of the latent representation of \mathbf{s} by the label, \mathbf{t} , via the conditional prior $p_{\psi}(\mathbf{z} | \mathbf{t})$ as well as the classifier $q_{\varphi}(\mathbf{t} | \mathbf{z})$.

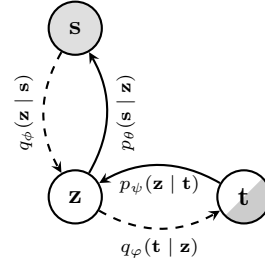


Figure 2: Simplified graphical model from Joy et al. (2021).

The corresponding objective for *supervised* data, derived as the (negative) variational free energy or evidence lower bound (ELBO) of the model is

$$\log p_{\theta,\psi}(\mathbf{s}, \mathbf{t}) \geq \mathcal{L}(\mathbf{s}, \mathbf{t}) = \mathbb{E}_{q_{\phi}(\mathbf{z}|\mathbf{s})} \left[\frac{q_{\phi}(\mathbf{t}|\mathbf{z})}{q_{\phi}(\mathbf{z}|\mathbf{s})} \log \frac{p_{\theta}(\mathbf{s}|\mathbf{z})p_{\psi}(\mathbf{z}|\mathbf{t})}{q_{\phi}(\mathbf{z}|\mathbf{s})q_{\phi}(\mathbf{t}|\mathbf{z})} \right] + \log q_{\phi,\varphi}(\mathbf{t}|\mathbf{s}) + \log p(\mathbf{t}). \quad (1)$$

A derivation of this objective can be found in Appendix A.

3.2 Mutual Supervision

Procedurally, a semi-supervised VAE is already multimodal. Beyond viewing labels as a separate data modality, for more typical multimodal data (vision, language), one would just need to replace labels with data from the appropriate modality, and adjust the corresponding encoder and decoder to handle such data. Conceptually however, this simple replacement can be problematic.

Supervised learning encapsulates a very specific imbalance in information between observed data and the labels—that labels do not encode information beyond what is available in the observation itself. This is a consequence of the fact that labels are typically characterised as projections of the data into some lower-dimensional conceptual subspace such as the set of object classes one may encounter in images, for example. Such projections cannot introduce additional information into the system, implying that the information in the data subsumes the information in the labels, i.e. that the conditional entropy of label \mathbf{t} given data \mathbf{s} is zero: $H(\mathbf{t} | \mathbf{s}) = 0$. Supervision-based models typically incorporate this information imbalance as a feature, as observed in the specific correspondences and structuring enforced between their label \mathbf{y} and latent \mathbf{z} in Joy et al. (2021).

Multimodal data of the kind considered here, on the other hand, does not exhibit this feature. Rather than being characterised as a projection from one modality to another, they are better understood as idiosyncratic projections of an abstract concept into distinct modalities—for example, as an image of a bird or a textual description of it. In this setting, no one modality has *all* the information, as each modality can encode unique perspectives opaque to the other. More formally, this implies that both the conditional entropies $H(\mathbf{t} | \mathbf{s})$ and $H(\mathbf{s} | \mathbf{t})$ are finite.

Based on this insight we symmetrise the semi-supervised VAE formulation by additionally constructing a mirrored version, with \mathbf{s}, \mathbf{t} swapped along with their corresponding parameters. This has the effect of also incorporating the information flow in the opposite direction to the standard case as $\mathbf{t} \rightarrow \mathbf{z} \rightarrow \mathbf{s}$, ensuring that the modalities are now *mutually supervised*. Extending the semi-supervised VAE objective (1), we construct a bi-directional objective for MEME

$$\mathcal{L}_{\text{Bi}}(\mathbf{s}, \mathbf{t}) = \frac{1}{2} [\mathcal{L}(\mathbf{s}, \mathbf{t}) + \mathcal{L}(\mathbf{t}, \mathbf{s})], \quad (2)$$

where both information flows are weighted equally. On a practical note, we find that it is important to ensure that parameters are shared appropriately when mirroring the terms, and that the variance in the gradient estimator is controlled effectively. Please see Appendices C and D for further details.

3.3 Learning from Partial Observations

In practice, prohibitive costs on multimodal data collection and curation imply that observations can frequently be partial, i.e., have missing modalities. One of the main benefits of the method introduced here is its natural extension to the case of partial observations on account of its semi-supervised underpinnings. Consider, without loss of generality, the case where we observe modality \mathbf{s} , but not its pair \mathbf{t} . Recalling the autoregressive generative model $p(\mathbf{s}, \mathbf{z}, \mathbf{t}) = p(\mathbf{s} | \mathbf{z})p(\mathbf{z} | \mathbf{t})p(\mathbf{t})$ we can derive a lower bound on the log-evidence

$$\log p_{\theta,\psi}(\mathbf{s}) = \log \int p_{\theta}(\mathbf{s} | \mathbf{z})p_{\psi}(\mathbf{z} | \mathbf{t})p(\mathbf{t}) d\mathbf{z} d\mathbf{t} \geq \mathbb{E}_{q_{\phi}(\mathbf{z}|\mathbf{s})} \left[\log \frac{p_{\theta}(\mathbf{s} | \mathbf{z}) \int p_{\psi}(\mathbf{z} | \mathbf{t})p(\mathbf{t}) d\mathbf{t}}{q_{\phi}(\mathbf{z} | \mathbf{s})} \right]. \quad (3)$$

Estimating the integral $p(\mathbf{z}) = \int p(\mathbf{z} | \mathbf{t})p(\mathbf{t}) d\mathbf{t}$ highlights another conceptual difference between a (semi-)supervised setting and a multimodal one. When \mathbf{t} is seen as a label, this typically implies that one could possibly compute the integral *exactly* by explicit marginalisation over its support, or at the very least, construct a reasonable estimate through simple Monte-Carlo integration. In Joy et al. (2021), the authors extend the latter approach through importance sampling with the “inner” encoder $q(\mathbf{t} | \mathbf{z})$, to construct a looser lower bound to (3).

In the multimodal setting however, this poses serious difficulties as the domain of the variable \mathbf{t} is not simple categorical labels, but rather complex continuous-valued data. This rules out exact marginalisation, and renders further importance-sampling practically infeasible on account of the quality of samples one can expect from the encoder $q(\mathbf{t} | \mathbf{z})$ which itself is being learnt from data. To overcome this issue, we adopt an optimisation approach inspired by the variational mixture of posteriors (VAMP) model introduced by Tomczak and Welling (2018).

Noting that our model formulation includes a conditional prior $p_\psi(\mathbf{z} | \mathbf{t})$, we introduce a set of N learnable pseudo-samples $\mathbf{u}_i^t, i = 1, \dots, N$ (collectively denoted λ_t) to estimate the prior $p(\mathbf{z})$ as a mixture over these values $p_{\lambda_t}(\mathbf{z}) = \frac{1}{N} \sum_{i=1}^N p_\psi(\mathbf{z} | \mathbf{u}_i^t)$. Our objective for unobserved data is thus

$$\mathcal{L}(\mathbf{s}) = \mathbb{E}_{q_\phi(\mathbf{z}|\mathbf{s})} \left[\log \frac{p_\theta(\mathbf{s} | \mathbf{z}) p_{\lambda_t}(\mathbf{z})}{q_\phi(\mathbf{z} | \mathbf{s})} \right] = \mathbb{E}_{q_\phi(\mathbf{z}|\mathbf{s})} \left[\log \frac{p_\theta(\mathbf{s} | \mathbf{z})}{q_\phi(\mathbf{z} | \mathbf{s})} + \log \frac{1}{N} \sum_{i=1}^N p_\psi(\mathbf{z} | \mathbf{u}_i^t) \right]. \quad (4)$$

For a dataset \mathcal{D} containing partial observations the overall objective (to maximise) becomes

$$\sum_{\mathbf{s}, \mathbf{t} \in \mathcal{D}} \log p_{\theta, \psi}(\mathbf{s}, \mathbf{t}) \geq \sum_{\mathbf{s} \in \mathcal{D}_s} \mathcal{L}(\mathbf{s}) + \sum_{\mathbf{t} \in \mathcal{D}_t} \mathcal{L}(\mathbf{t}) + \sum_{\mathbf{s}, \mathbf{t} \in \mathcal{D}_{s,t}} \mathcal{L}_{\text{Bi}}(\mathbf{s}, \mathbf{t}), \quad (5)$$

This treatment of unobserved data distinguishes our approach from alternatives such as that of Shi et al. (2019), where model updates for missing modalities are infeasible. Whilst there is the possibility to perform multimodal learning in the weakly supervised case as introduced by Wu and Goodman (2018), their approach directly affects the posterior distribution, whereas ours only affects the regularization of the embedding during training. At test time, Wu and Goodman (2018) will produce different embeddings depending on whether all modalities are present, which is typically at odds with the concept of placing the embeddings of related modalities in the same region of the latent space. Our approach does not suffer from this issue as the posterior remains unchanged regardless of whether the other modality is present or not.

Learning with MEME Given the overall objective in (5), we train MEME through maximum-likelihood estimation of the objective over a dataset \mathcal{D} . Each observation from the dataset is optimised using the relevant term in the right-hand side of (5), through the use of standard stochastic gradient descent methods. Note that training the objective involves learning *all* the (neural network) parameters $(\theta, \psi, \phi, \varphi)$ in the fully-observed, bi-directional case. When training with a partial observation, say just \mathbf{s} , all parameters except the relevant likelihood parameter φ (for $q_\varphi(\mathbf{t} | \mathbf{z})$) are learnt. Note that the encoding for data in the domain of \mathbf{t} is still computed through the learnable pseudo-samples \mathbf{u}_t , denoted collectively as λ_t . This is reversed when training on an observation with just \mathbf{t} .

Generalisation beyond two modalities Here, we develop our method by confining our attention to the bi-modal case. We believe this to be a reasonable stance for two important reasons. Firstly, the number of modalities one typically encounters in the multimodal setting is fairly small to begin with. This is often a consequence of its parallels with embodied perception, where one is restricted by the relatively small number of senses available such as sight, sound, and proprioception. Furthermore, the vast majority of work on multimodal VAEs only really consider the bimodal setting, as evidenced by the prior work discussed earlier (§ 2). Secondly, it is in fact quite straightforward to extend MEME to settings beyond the bimodal case, by simply incorporating existing explicit combinations (e.g. mixtures or products) *on top of* the implicit combination discussed here. Our focus in this work lies in exploring and analysing the utility of implicit combination in the multimodal setting, and our formulation and experiments reflect this focus.

4 Experiments

4.1 Learning from Partially Observed Data

In this section, we evaluate the performance of MEME following standard multimodal VAE metrics as proposed in Shi et al. (2019). The two metrics we selected are *cross coherence* to evaluate the semantic quality of reconstruction, as well as *latent accuracy* in a classification task to examine the representation learnt in the latent space. Notably, since our model benefits from its implicit latent regularisation and is able to learn from partially-observed data, we evaluate MEME’s performance on the two metrics when different proportions of data are missing in either or both modalities. We



Figure 3: MEME cross-modal generations for MNIST-SVHN.

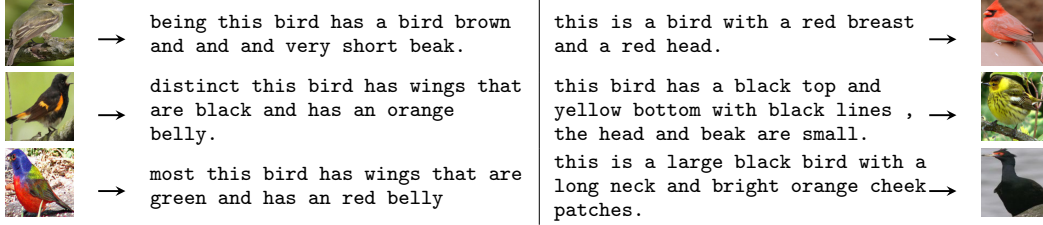


Figure 4: MEME cross-modal generations for CUB.

demonstrate our results on two datasets, namely an image \leftrightarrow image dataset MNIST-SVHN (LeCun et al., 2010; Netzer et al., 2011) and an image \leftrightarrow caption dataset CUB (Welinder et al., 2010).

Cross Coherence Here, we focus mainly on the models’ ability to reconstruct in one modality, say, t , given another modality s as input, while preserving the conceptual commonality between the two. Following Massiceti et al. (2018); Shi et al. (2019), we report the cross coherence score on MNIST-SVHN as the percentage of matching digits in the input and output modality, and on CUB we perform canonical correlation analysis (CCA) on input-output pairs of cross generation to measure the correlation between these samples.

In Figure 5 we plot the cross coherence for MNIST-SVHN and display the correlation results for CUB in Figure 6, across different partial-observation schemes. The x-axis represents the proportion of data that is paired, while the subscript to the method (see legends) indicates the modality that is presented. For instance, MEME_MNIST with $f = 0.25$ indicates that only 25% of samples are paired, and the other 75% only contain MNIST digits, and MEME_SPLIT with $f = 0.25$ indicates that the 75% contains a mix of MNIST and SVHN samples that are unpaired and never observed together, i.e we alternate depending on the iteration. We provide qualitative results in Figure 3 and Figure 4.

We can see that our model is able to obtain higher coherence scores than baselines including MVAE (Wu and Goodman, 2018) and MMVAE (Shi et al., 2019) in the fully observed case where $f = 1.0$. This holds true for both MNIST-SVHN and CUB. We note that some of the reported results of MMVAE in our experiments are worse than those seen in the original paper. This is because MVAE is restricted to using Gaussian distributions for the posterior and prior, and therefore we adopt Gaussian posteriors and priors for all three models to ensure like-for-like comparison. Better results for MMVAE can be obtained with Laplace posteriors and priors, and we provide a comparison between MEME and MMVAE under this setting in Appendix G.

As the percentage of observed pairs f decreases, the performance of MEME drops gradually, however stays consistently higher than MVAE. We did not include results for MMVAE where $f < 1.0$ as the model does not handle partial observations at train time.

It is interesting to see that cross-generating MNIST obtains a similar performance depending on whether we partially observe MNIST or SVHN. The same is not true for MNIST \rightarrow SVHN, where we see a dramatic decrease in coherence scores when partially observing MNIST. We posit that this is because the information needed to generate an MNIST digit is typically sub-summed within an SVHN digit (e.g. there is little style information associated with MNIST), making generation from SVHN to MNIST easier, and from MNIST to SVHN more difficult.

In Figure 6 we can see that MEME consistently obtains higher correlations than MVAE across all supervision rates, and higher than MMVAE in the fully supervised case. Generally, cross-generating images yields higher correlation values, possibly due to the difficulty in generating semantically meaningful text with relatively simplistic convolutional architectures. We would like to highlight that fully observing images typically leads to poorer performance when cross-generating captions. Again, possibly due to the difficulty in generating text, but also possibly due to a discord between how the latent space is structured, where a similar pattern emerged when MNIST was only partially observed.

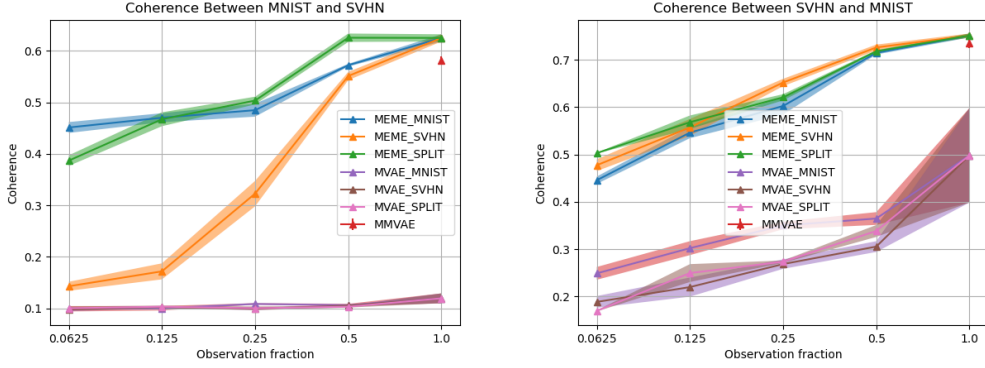


Figure 5: Coherence between MNIST and SVHN (Left) and SVHN and MNIST (Right). Shaded area indicates one-standard deviation of runs with different seeds.

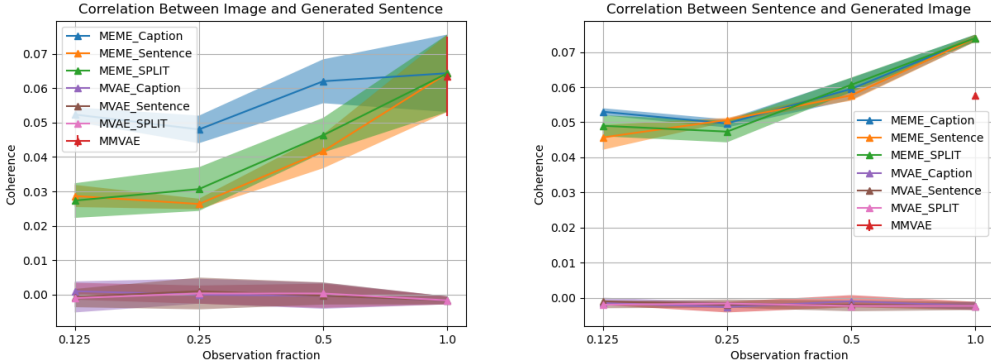


Figure 6: Correlation between Image and Sentence (Left) and Sentence and Image (Right). Shaded area indicates one-standard deviation of runs with different seeds.

Latent Accuracy We also conduct experiments to evaluate the quality of representation learnt in the latent space. Again, following the practice in Shi et al. (2019), we fit a linear classifier to the latent samples and compute the classification accuracy of predicting the input digit. The intuition is that if a linear classifier can extract digit information from the latents, it indicates the presence of a linear subspace that is structured according to the underlying class.

See results in Figure 7. Similar to our findings in cross coherence, MEME outperforms baselines under *both* fully observed ($f = 1.0$) but for the partially observed ($f < 1.0$) setting it seems to perform worse than MVAE when classifying MNIST. However, we note that MVAE fails from a coherence perspective, indicating that it just optimises the latent space. However, we do notice that MVAE_SPLIT seems to structure the latent space appropriately for MNIST, we posit that this is due to the sub-sampling regime. Typically, given an SVHN image we obtain lower classification accuracies than if we were given an MNIST image potentially due to the lack of structuring naturally occurring from SVHN. We also see here that fully observing MNIST actually improves the classification score for SVHN than if we fully observe SVHN; due to the presence of MNIST causing the latent space to structure in a more suitable way for classification.

In this section, we demonstrated the strong performance of MEME given both fully observed and partially observed multimodal data. Our method outperformed two state-of-the-art multimodal VAEs (MVAE and MMVAE) consistently on two challenging multimodal datasets. Importantly, our method performed well under different missingness mechanisms. As demonstrated in the experiments, it learns from partially observed data when 1) data from one of the modalities is missing and 2) evenly split, unpaired multimodal data is given to the model. Compared to prior work, such as Shi et al. (2021), that only improves data efficiency when evenly split, unpaired multimodal data is provided, our method is more generally applicable.

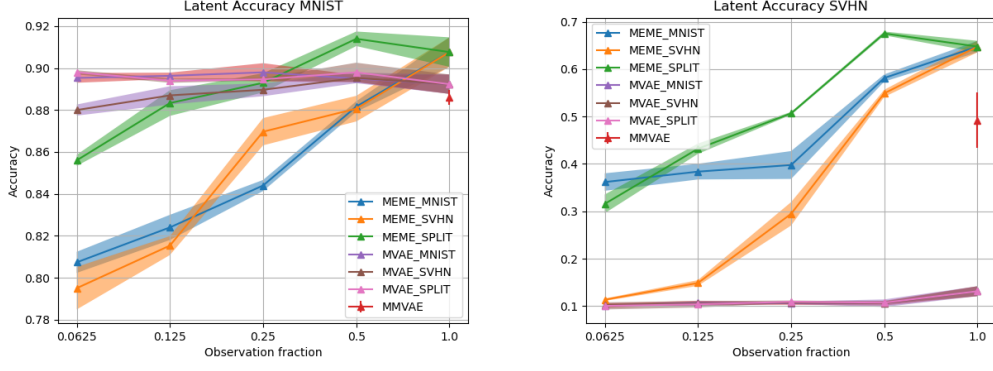


Figure 7: Latent accuracies for MNIST and SVHN (Left) and SVHN and MNIST (Right). Shaded area indicates one-standard deviation of runs with different seeds.

4.2 Evaluating Relatedness

Now that we have established that the representation learned by MEME contains rich class information from the inputs, we also wish to analyse the relationship between the encodings of different modalities by studying their “relatedness”, i.e. semantic similarity. The probabilistic nature of the learned representations suggests the use of probability distance functions as a measure of relatedness, where a low distance implies closely related representations and vice versa.

In the following experiments we use the 2-Wasserstein distance, \mathcal{W}_2 , a probability metric with a closed-form expression for Gaussian distributions (see Appendix E for more details). Specifically, we compute $d_{ij} = \mathcal{W}_2(q(\mathbf{z}|\mathbf{s}_i) \parallel q(\mathbf{z}|\mathbf{t}_j))$, where $q(\mathbf{z}|\mathbf{s}_i)$ and $q(\mathbf{z}|\mathbf{t}_j)$ are the individual encoders, for all combination of pairs $\{\mathbf{s}_i, \mathbf{t}_j\}$ in the mini-batch, i.e. $\{\mathbf{s}_i, \mathbf{t}_j\}$, for $i, j \in \{1 \dots M\}$ where M is the number of elements in the mini-batch.

General Relatedness In this experiment we wish to highlight the disparity in measured relatedness between paired vs. unpaired multimodal data. To do so, we plot d_{ij} on a histogram and color-code the histogram by whether the corresponding data pair $\{\mathbf{s}_i, \mathbf{t}_j\}$ shows the same concept, e.g. same digit for MNIST-SVHN and same image-caption pair for CUB. Ideally, we should observe smaller

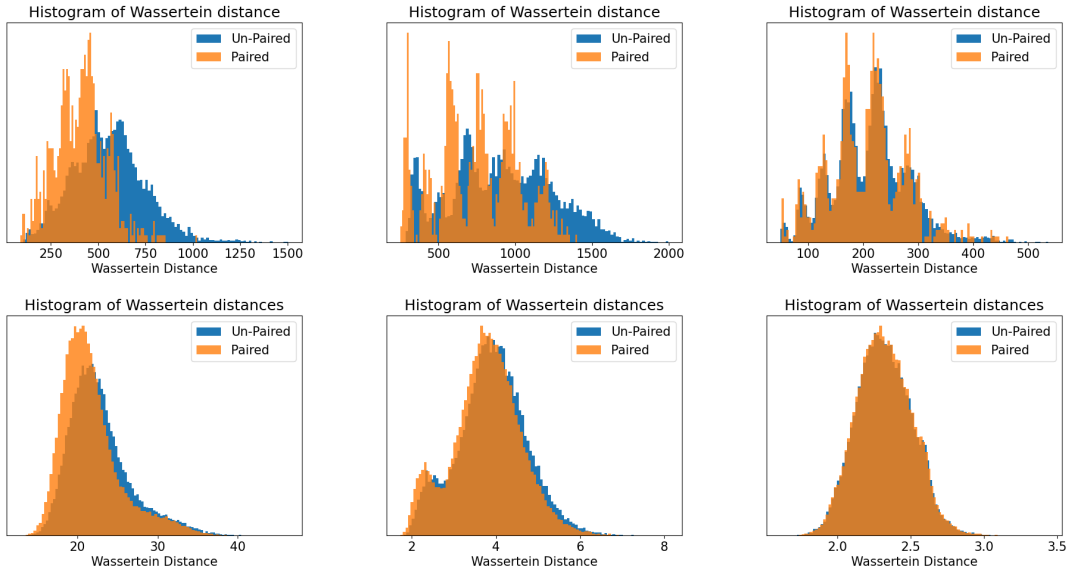


Figure 8: Histograms of Wassertein distance for SVHN and MNIST (Top) and CUB (Bottom): MEME (Left), MMVAE (middle) and MVAE (Right). Blue indicates *unpaired* samples and orange *paired* samples. We expect to see high densities of blue at further distances and visa-versa for orange.

distances between encoding distributions for data pairs that are related, and larger for ones that are not.

In Figure 8, we see that MEME (left) yields higher mass at lower distance values for paired multimodal samples compared to MMVAE and MVAE (middle/right column) than it does for unpaired ones, featuring larger disparity in encoding distances between paired and unpaired instances. This demonstrates MEME’s capability of capturing relatedness between multimodal samples in its latent space, and further showcased its ability to learn good quality representation.

Class-contextual Relatedness To offer more insights on the relatedness of representations within classes, we construct a distance matrix $\mathbf{K} \in \mathbb{R}^{10 \times 10}$ for the MNIST-SVHN dataset, where each element $\mathbf{K}_{i,j}$ corresponds to the average \mathcal{W}_2 distance between encoding distributions of class i of MNIST and j of SVHN. A perfect distance matrix will consist of a diagonal of all zeros and positive values in the off-diagonal.

See the class distance matrix in Figure 9 (top row), generated with models trained on fully observed multimodal data. It is clear that our model (left) produces much lower distances on the diagonal, i.e. when input classes for the two modalities are the same, and higher distances off diagonal where input classes are different. A clear, lower-valued diagonal can also be observed for MMVAE (middle), however it is less distinct compared to MEME, since some of the mismatched pairs also obtains smaller values. The distance matrix for MVAE (right), on the other hand, does not display a diagonal at all, reflecting poor ability to identify relatedness or extract class information through the latent.

To closely examine which digits are considered similar by the model, we construct dendrograms to visualise the hierarchical clustering of digits by relatedness, as seen in Figure 9 (bottom row). We see that our model (left) is able to obtain a clustering of conceptually similar digits. In particular, digits with smoother writing profile such as 3, 5, 8, along with 6 and 9 are clustered together (right hand side of dendrogram), and the digits with sharp angles, such as 4 and 7 are clustered together. The same trend is not observed for MMVAE nor MVAE. It is also important to note the height of each bin, where higher values indicate greater distance between clusters. Generally the clusters obtained in MEME are further separated for MMVAE, demonstrating more distinct clustering across classes.

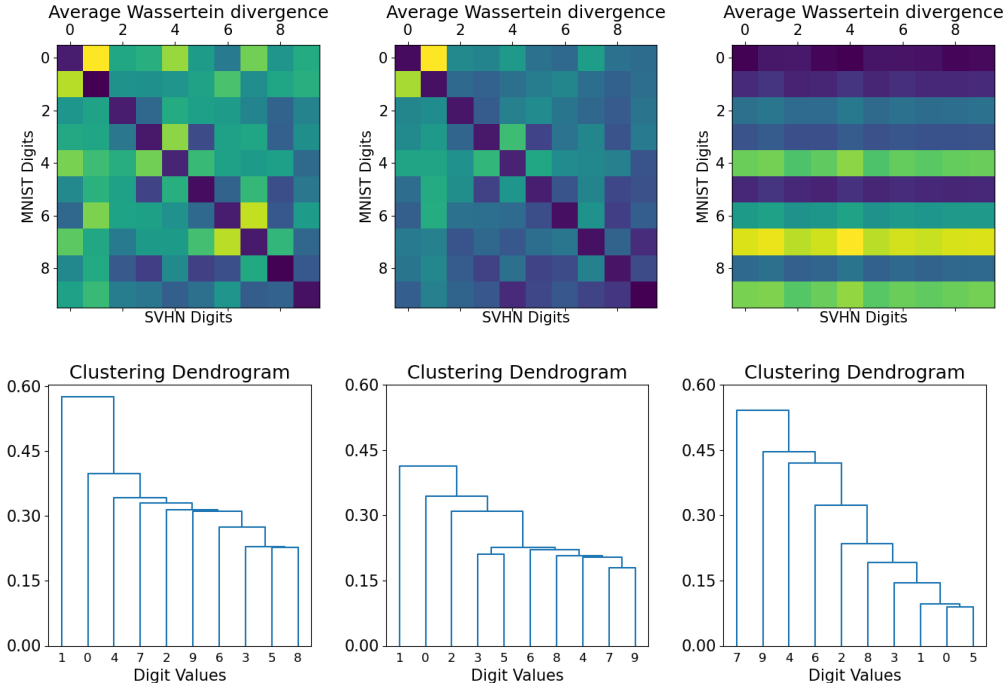


Figure 9: Distance matrices for KL divergence between classes for SVHN and MNIST (Top) and dendrogram (Bottom) for: Ours (Left), MVAE (middle) and MMVAE (Right).

5 Discussion

Here we have presented a method which faithfully deals with partially observed modalities in VAEs. Through leveraging recent advances in semi-supervised VAEs, we construct a model which is amenable to multi-modal learning when modalities are partially observed. Specifically, our method employs mutual supervision by treating the uni-modal encoders individually and minimizing a KL between them to ensure embeddings for are pertinent to one another. This approach enables us to successfully learn a model when either of the modalities are partially observed. Furthermore, our model is able to naturally extract an indication of relatedness between modalities. We demonstrate our approach on the MNIST-SVHN and CUB datasets, where training is performed on a variety of different observations rates.

References

- Y. Gal. *Uncertainty in deep learning*. PhD thesis, University of Cambridge, 2016. Unpublished doctoral dissertation.
- S. Ghalebikesabi, R. Cornish, C. Holmes, and L. J. Kelly. Deep generative missingness pattern-set mixture models. In *AISTATS*, pages 3727–3735, 2021.
- C. R. Givens and R. M. Shortt. A class of Wasserstein metrics for probability distributions., 2002. ISSN 0026-2285.
- Y. Gong, H. Hajimirsadeghi, J. He, T. Durand, and G. Mori. Variational selective autoencoder: Learning from partially-observed heterogeneous data. In *AISTATS*, pages 2377–2385, 2021.
- O. Ivanov, M. Figurnov, and D. P. Vetrov. Variational autoencoder with arbitrary conditioning. In *International Conference on Learning Representations*, pages 1–25, 2019.
- T. Joy, S. Schmon, P. Torr, S. N, and T. Rainforth. Capturing label characteristics in {vae}s. In *International Conference on Learning Representations*, 2021. URL <https://openreview.net/forum?id=wQR1SUZ5V7B>.
- D. P. Kingma and M. Welling. Auto-encoding variational bayes. In *International Conference on Learning Representations*, 2014.
- Y. LeCun, C. Cortes, and C. Burges. Mnist handwritten digit database. *ATT Labs [Online]*. Available: <http://yann.lecun.com/exdb/mnist>, 2, 2010.
- C. Ma, S. Tschitschek, K. Palla, J. M. Hernández-Lobato, S. Nowozin, and C. Zhang. Eddi: Efficient dynamic discovery of high-value information with partial vae. In *International Conference on Machine Learning*, pages 4234–4243, 2018.
- D. Massiceti, N. Siddharth, P. K. Dokania, and P. H. Torr. FlipDial: a generative model for two-way visual dialogue. In *IEEE Conference on Computer Vision and Pattern Recognition*, 2018.
- P.-A. Mattei and J. Frellsen. Miwae: Deep generative modelling and imputation of incomplete data sets. In *International Conference on Machine Learning*, pages 4413–4423, 2019.
- A. Nazábal, P. M. Olmos, Z. Ghahramani, and I. Valera. Handling incomplete heterogeneous data using vaes. *Pattern Recognition*, 107:107501, 2020.
- Y. Netzer, T. Wang, A. Coates, A. Bissacco, B. Wu, and A. Y. Ng. Reading digits in natural images with unsupervised feature learning. 2011.
- Y. Shi, N. Siddharth, B. Paige, and P. H. Torr. Variational mixture-of-experts autoencoders for multi-modal deep generative models. *arXiv*, (NeurIPS), 2019. ISSN 23318422. URL <https://arxiv.org/pdf/1911.03393.pdf>.
- Y. Shi, B. Paige, P. Torr, and S. N. Relating by contrasting: A data-efficient framework for multimodal generative models. In *ICLR 2021: The Ninth International Conference on Learning Representations*, 2021.
- N. Siddharth, T. B. Paige, J.-W. Van de Meent, A. Desmaison, N. Goodman, P. Kohli, F. Wood, and P. Torr. Learning disentangled representations with semi-supervised deep generative models. In *Advances in Neural Information Processing Systems*, pages 5925–5935, 2017.
- L. Smith and Y. Gal. Understanding measures of uncertainty for adversarial example detection. *arXiv preprint arXiv:1803.08533*, 2018.
- T. M. Sutter, I. Daunhawer, and J. E. Vogt. Multimodal generative learning utilizing jensen-shannon divergence. In *Workshop on Visually Grounded Interaction and Language at the 33rd Conference on Neural Information Processing Systems (NeurIPS 2019)*, volume 33, pages 6100–6110, 2020.
- T. M. Sutter, I. Daunhawer, and J. E. Vogt. Generalized multimodal elbo. In *ICLR 2021: The Ninth International Conference on Learning Representations*, 2021.

- M. Suzuki, K. Nakayama, and Y. Matsuo. Joint multimodal learning with deep generative models. In *International Conference on Learning Representations Workshop*, 2016.
- J. M. Tomczak and M. Welling. VAE with a vampprior. *Proceedings of Machine Learning Research*, 2018.
- Y. H. Tsai, P. P. Liang, A. A. Bagherzade, L.-P. Morency, and R. Salakhutdinov. Learning factorized multimodal representations. In *International Conference on Learning Representations*, 2019.
- R. Vedantam, I. Fischer, J. Huang, and K. Murphy. Generative models of visually grounded imagination. In *International Conference on Learning Representations*, 2018.
- P. Welinder, S. Branson, T. Mita, C. Wah, F. Schroff, S. Belongie, and P. Perona. Caltech-UCSD Birds 200. Technical Report CNS-TR-2010-001, California Institute of Technology, 2010.
- M. Wu and N. Goodman. Multimodal generative models for scalable weakly-supervised learning. *Adv. Neural Inf. Process. Syst.*, 2018-Decem(Nips):5575–5585, 2018. ISSN 10495258. URL <https://arxiv.org/pdf/1802.05335.pdf>.

Checklist

1. For all authors...
 - (a) Do the main claims made in the abstract and introduction accurately reflect the paper’s contributions and scope? [Yes]
 - (b) Did you describe the limitations of your work? [Yes] see discussion in § 3.3
 - (c) Did you discuss any potential negative societal impacts of your work? [N/A] This work discusses repurposing semi-supervised VAEs for multimodal data.
 - (d) Have you read the ethics review guidelines and ensured that your paper conforms to them? [Yes]
2. If you ran experiments...
 - (a) Did you include the code, data, and instructions needed to reproduce the main experimental results (either in the supplemental material or as a URL)? [No] Code will be made publicly available at a later date.
 - (b) Did you specify all the training details (e.g., data splits, hyperparameters, how they were chosen)? [Yes] see ??
 - (c) Did you report error bars (e.g., with respect to the random seed after running experiments multiple times)? [Yes]
 - (d) Did you include the total amount of compute and the type of resources used (e.g., type of GPUs, internal cluster, or cloud provider)? [Yes] see ??
3. If you are using existing assets (e.g., code, data, models) or curating/releasing new assets...
 - (a) If your work uses existing assets, did you cite the creators? [Yes]
 - (b) Did you mention the license of the assets? [Yes] All datasets are publicly available.
 - (c) Did you include any new assets either in the supplemental material or as a URL? [No]
 - (d) Did you discuss whether and how consent was obtained from people whose data you’re using/curating? [N/A]
 - (e) Did you discuss whether the data you are using/curating contains personally identifiable information or offensive content? [N/A]

A Derivation of the Objective

The variational lower bound for the case when \mathbf{s} and \mathbf{t} are both observed derives as:

$$\begin{aligned}\log p(\mathbf{t}, \mathbf{s}) &= \log \int_{\mathbf{z}} p(\mathbf{t}, \mathbf{s}, \mathbf{z}) d\mathbf{z} \\ &\geq \int_{\mathbf{z}} \log \frac{p(\mathbf{s}, \mathbf{t}, \mathbf{z})}{q(\mathbf{z}|\mathbf{t}, \mathbf{s})} q(\mathbf{z}|\mathbf{t}, \mathbf{s}) d\mathbf{z}\end{aligned}$$

Following Joy et al. (2021), assuming $\mathbf{s} \perp\!\!\!\perp \mathbf{t}|\mathbf{z}$ and applying Bayes rule we have

$$q(\mathbf{z}|\mathbf{t}, \mathbf{s}) = \frac{q(\mathbf{z}|\mathbf{s})q(\mathbf{t}|\mathbf{z})}{q(\mathbf{t}|\mathbf{s})}, \quad (6)$$

which can be substituted into the lower bound to obtain

$$\begin{aligned}\log p(\mathbf{t}, \mathbf{s}) &\geq \int_{\mathbf{z}} \log \frac{p(\mathbf{s}, \mathbf{t}, \mathbf{z})q(\mathbf{t}|\mathbf{s})}{q(\mathbf{z}|\mathbf{s})q(\mathbf{t}|\mathbf{z})} \frac{q(\mathbf{z}|\mathbf{s})q(\mathbf{t}|\mathbf{z})}{q(\mathbf{t}|\mathbf{s})} d\mathbf{z} \\ &= \mathbb{E}_{q(\mathbf{z}|\mathbf{s})} \left[\frac{q(\mathbf{t}|\mathbf{z})}{q(\mathbf{t}|\mathbf{s})} \log \frac{p(\mathbf{s}|\mathbf{z})p(\mathbf{z}|\mathbf{t})}{q(\mathbf{z}|\mathbf{s})q(\mathbf{t}|\mathbf{z})} \right] + \log q(\mathbf{t}|\mathbf{s}) + \log p(\mathbf{t}).\end{aligned}$$

B High Variance of the gradient estimator

During training, the term $\frac{q(\mathbf{t}|\mathbf{z})}{q(\mathbf{t}|\mathbf{s})}$ introduces a very low signal to noise ratio. To combat this issue, we modify the gradient of the objective, enabling us to learn meaningful parameters.

The gradient of the first term in the objective wrt ϕ is given as

$$\begin{aligned}\nabla_{\phi} \mathcal{L}(\mathbf{s}, \mathbf{t}; \phi, \varphi, \theta, \vartheta) &= \mathbb{E}_{p(\epsilon)} \left\{ \nabla_{\phi} \left[\frac{q(\mathbf{t}|\mathbf{z})}{q(\mathbf{t}|\mathbf{s})} \right] \log \frac{p(\mathbf{s}|\mathbf{z})p(\mathbf{z}|\mathbf{t})p(\mathbf{t})}{q(\mathbf{z}|\mathbf{s})q(\mathbf{t}|\mathbf{z})} \right. \\ &\quad \left. + \left[\frac{q(\mathbf{t}|\mathbf{z})}{q(\mathbf{t}|\mathbf{s})} \right] \nabla_{\phi} \log \frac{p(\mathbf{s}|\mathbf{z})p(\mathbf{z}|\mathbf{t})p(\mathbf{t})}{q(\mathbf{z}|\mathbf{s})q(\mathbf{t}|\mathbf{z})} \right\},\end{aligned} \quad (7)$$

with $\mathbf{z} = t(\epsilon, \mathbf{s}; \phi)$, using the reparameterization trick as usual. Here we observe that the first term has a variance which is too high to learn anything meaningful from. Fortunately, we note that, under certain conditions, the expected value of the first term is zero. Consequently, we simply remove this gradient component from the objective, which can easily be achieved by introducing a stop gradient on the $\frac{q(\mathbf{t}|\mathbf{z})}{q(\mathbf{t}|\mathbf{s})}$ term.

Using the reparameterisation trick, with $\mathbf{z} = t(\epsilon)$ for convenience, the first term of (7) can be expanded as

$$\mathbb{E}_{\epsilon \sim g(\epsilon)} \left[\frac{\int q_{\varphi}(\mathbf{t} | \mathbf{z}) q_{\phi}(\mathbf{z} | \mathbf{s}) d\mathbf{z} \nabla_{\mathbf{z}} q_{\varphi}(\mathbf{t}|\mathbf{z}) \nabla_{\phi} t(\epsilon)}{[\int q_{\varphi}(\mathbf{t} | \mathbf{z}) q_{\phi}(\mathbf{z} | \mathbf{s}) d\mathbf{z}]^2} \log \frac{p_{\theta}(\mathbf{s}|\mathbf{z})p_{\vartheta}(\mathbf{z}|\mathbf{t})}{q_{\varphi}(\mathbf{t}|\mathbf{z})q_{\phi}(\mathbf{z}|\mathbf{s})} \right] \quad (8)$$

$$- \mathbb{E}_{\epsilon \sim g(\epsilon)} \left[\frac{q_{\varphi}(\mathbf{t}|\mathbf{z}) \nabla_{\phi} \int q_{\varphi}(\mathbf{t} | \mathbf{z}) q_{\phi}(\mathbf{z} | \mathbf{s}) d\mathbf{z}}{[\int q_{\varphi}(\mathbf{t} | \mathbf{z}) q_{\phi}(\mathbf{z} | \mathbf{s}) d\mathbf{z}]^2} \log \frac{p_{\theta}(\mathbf{s}|\mathbf{z})p_{\vartheta}(\mathbf{z}|\mathbf{t})}{q_{\varphi}(\mathbf{t}|\mathbf{z})q_{\phi}(\mathbf{z}|\mathbf{s})} \right]$$

$$\mathbb{E}_{\epsilon \sim g(\epsilon)} \left[\frac{\int q_{\varphi}(\mathbf{t} | \mathbf{z}) q_{\phi}(\mathbf{z} | \mathbf{s}) d\mathbf{z} \nabla_{\mathbf{z}} q_{\varphi}(\mathbf{t}|\mathbf{z}) \nabla_{\phi} t(\epsilon)}{[\int q_{\varphi}(\mathbf{t} | \mathbf{z}) q_{\phi}(\mathbf{z} | \mathbf{s}) d\mathbf{z}]^2} \log \frac{p_{\theta}(\mathbf{s}|\mathbf{z})p_{\vartheta}(\mathbf{z}|\mathbf{t})}{q_{\varphi}(\mathbf{t}|\mathbf{z})q_{\phi}(\mathbf{z}|\mathbf{s})} \right] \quad (9)$$

$$- \mathbb{E}_{\epsilon \sim g(\epsilon)} \left[\frac{q_{\varphi}(\mathbf{t}|\mathbf{z}) \nabla_{\phi} \int q_{\varphi}(\mathbf{t}|\mathbf{z}') g(\alpha) d\alpha}{[\int q_{\varphi}(\mathbf{t} | \mathbf{z}) q_{\phi}(\mathbf{z} | \mathbf{s}) d\mathbf{z}]^2} \log \frac{p_{\theta}(\mathbf{s}|\mathbf{z})p_{\vartheta}(\mathbf{z}|\mathbf{t})}{q_{\varphi}(\mathbf{t}|\mathbf{z})q_{\phi}(\mathbf{z}|\mathbf{s})} \right]$$

with $\mathbf{z}' = t(\alpha)$

$$\mathbb{E}_{\epsilon \sim g(\epsilon)} \left[\frac{\int q_{\varphi}(\mathbf{t}|t(\alpha)) g(\alpha) d\alpha \nabla_{\mathbf{z}} q_{\varphi}(\mathbf{t}|\mathbf{z}) \nabla_{\phi} t(\epsilon)}{[\int q_{\varphi}(\mathbf{t} | \mathbf{z}) q_{\phi}(\mathbf{z} | \mathbf{s}) d\mathbf{z}]^2} \log \frac{p_{\theta}(\mathbf{s}|\mathbf{z})p_{\vartheta}(\mathbf{z}|\mathbf{t})}{q_{\varphi}(\mathbf{t}|\mathbf{z})q_{\phi}(\mathbf{z}|\mathbf{s})} \right] \quad (10)$$

$$- \mathbb{E}_{\epsilon \sim g(\epsilon)} \left[\frac{q_{\varphi}(\mathbf{t}|\mathbf{z}) \int \nabla_{\mathbf{z}'} q_{\varphi}(\mathbf{t}|\mathbf{z}') \nabla_{\phi} t(\alpha) d\alpha}{[\int q_{\varphi}(\mathbf{t} | \mathbf{z}) q_{\phi}(\mathbf{z} | \mathbf{s}) d\mathbf{z}]^2} \log \frac{p_{\theta}(\mathbf{s}|\mathbf{z})p_{\vartheta}(\mathbf{z}|\mathbf{t})}{q_{\varphi}(\mathbf{t}|\mathbf{z})q_{\phi}(\mathbf{z}|\mathbf{s})} \right]$$

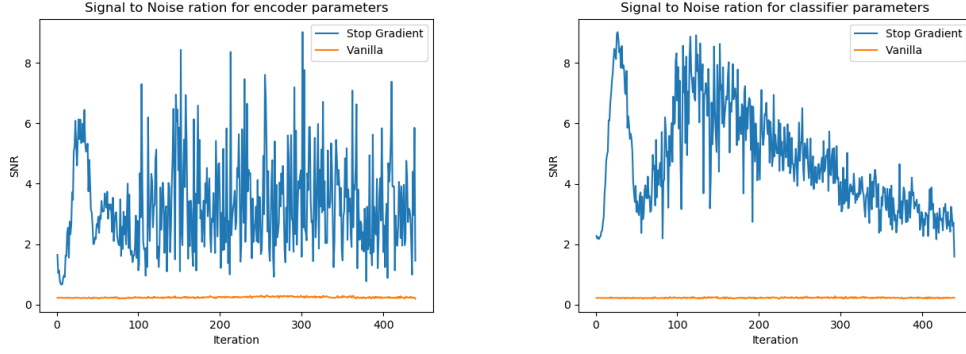


Figure 10: SNR for encoder parameters (Left) and classifier parameters (Right), blue indicates that we apply the stop gradient in Appendix B, orange indicates we do not. A higher value typically leads to improved learning.

$$\begin{aligned} & \int \mathbb{E}_{\epsilon \sim g(\epsilon)} \left[\frac{\int q_{\varphi}(\mathbf{t}|t(\alpha))g(\alpha)d\alpha \nabla_{\mathbf{z}} q_{\varphi}(\mathbf{t}|\mathbf{z}) \nabla_{\phi} t(\epsilon)}{[\int q_{\varphi}(\mathbf{t}|\mathbf{z})q_{\phi}(\mathbf{z}|\mathbf{s})d\mathbf{z}]^2} \log \frac{p_{\theta}(\mathbf{s}|\mathbf{z})p_{\vartheta}(\mathbf{z}|\mathbf{t})}{q_{\varphi}(\mathbf{t}|\mathbf{z})q_{\phi}(\mathbf{z}|\mathbf{s})} \right] d\alpha \\ & - \int \mathbb{E}_{\epsilon \sim g(\epsilon)} \left[\frac{q_{\varphi}(\mathbf{t}|\mathbf{z}) \int \nabla_{\mathbf{z}'} q_{\varphi}(\mathbf{t}|\mathbf{z}') \nabla_{\phi} t(\alpha) d\alpha}{[\int q_{\varphi}(\mathbf{t}|\mathbf{z})q_{\phi}(\mathbf{z}|\mathbf{s})d\mathbf{z}]^2} \log \frac{p_{\theta}(\mathbf{s}|\mathbf{z})p_{\vartheta}(\mathbf{z}|\mathbf{t})}{q_{\varphi}(\mathbf{t}|\mathbf{z})q_{\phi}(\mathbf{z}|\mathbf{s})} \right] d\alpha \end{aligned} \quad (11)$$

When the true posterior $p(\mathbf{z}|\mathbf{s})$ matches the approximate posterior $q_{\phi}(\mathbf{z}|\mathbf{s})$ and the predictive distribution $q_{\varphi}(\mathbf{t}|\mathbf{z})$ matches the true distribution $p(\mathbf{t}|\mathbf{z})$, by applying Bayes rule, the term inside the log is equivalent to $p(\mathbf{s})$, which is independent of ϵ and α .

$$\begin{aligned} & \int \int \left[\frac{q_{\varphi}(\mathbf{t}|g(\alpha))q(\alpha) \nabla_{g(\epsilon)} q_{\varphi}(\mathbf{t}|g(\epsilon)) \nabla_{\phi} g(\epsilon) q(\epsilon)}{[\int q_{\varphi}(\mathbf{t}|\mathbf{z})q_{\phi}(\mathbf{z}|\mathbf{s})d\mathbf{z}]^2} \right] d\epsilon d\alpha \log p(\mathbf{s}) \\ & - \int \int \left[\frac{q_{\varphi}(\mathbf{t}|g(\epsilon))q(\epsilon) \nabla_{g(\alpha)} q_{\varphi}(\mathbf{t}|g(\alpha)) \nabla_{\phi} g(\alpha) q(\alpha)}{[\int q_{\varphi}(\mathbf{t}|\mathbf{z})q_{\phi}(\mathbf{z}|\mathbf{s})d\mathbf{z}]^2} \right] d\epsilon d\alpha \log p(\mathbf{s}) \end{aligned} \quad (12)$$

Which subsequently equals zero, leading to our choice of removing this term from the gradient.

This modification can be viewed as the control variate strategy below

$$\hat{f}(\mathbf{z}) := f(\mathbf{z}) - \alpha(h(\mathbf{z}) - \mathbb{E}_{q_{\phi}(\mathbf{z}|\mathbf{s})}[h(\mathbf{z})]), \quad (13)$$

with $\alpha = 1$ and $\mathbb{E}[f(\mathbf{z})] = \mathbb{E}[\hat{f}(\mathbf{z})]$ as required. Here, the definitions of $f(\mathbf{z})$ and $h(\mathbf{z})$ are

$$f(\mathbf{z}) = \nabla_{\phi, \varphi} \mathbb{E}_{q(\mathbf{z}|\mathbf{s})} \left[\frac{q(\mathbf{t}|\mathbf{z})}{q(\mathbf{t}|\mathbf{s})} \log \frac{p(\mathbf{s}|\mathbf{z})p(\mathbf{z}|\mathbf{t})p(\mathbf{t})}{q(\mathbf{z}|\mathbf{s})q(\mathbf{t}|\mathbf{z})} \right] + \nabla_{\phi, \varphi} q_{\varphi, \phi}(\mathbf{t}|\mathbf{s}) \quad (14)$$

$$h(\mathbf{z}) = \nabla_{\phi, \varphi} \left[\frac{q(\mathbf{t}|\mathbf{z})}{q(\mathbf{t}|\mathbf{s})} \right] \log \frac{p(\mathbf{s}|\mathbf{z})p(\mathbf{z}|\mathbf{t})p(\mathbf{t})}{q(\mathbf{z}|\mathbf{s})q(\mathbf{t}|\mathbf{z})}. \quad (15)$$

We plot the resulting SNR ratios for the case when we apply the stop gradient (blue) and when do not (orange) in

C Weight Sharing

Another critical issue with naively training using (1), is that in certain situations $q_{\varphi}(\mathbf{t}|\mathbf{z})$ struggles to learn features (typically style) for \mathbf{t} , consequently making it difficult to generate realistic samples. This is due to the information entering the latent space only coming from \mathbf{s} , which contains all of the information needed to reconstruct \mathbf{s} , but does not necessarily contain the information needed to reconstruct a corresponding \mathbf{t} . Consequently, the term $p_{\theta}(\mathbf{s}|\mathbf{z})$ will learn appropriate features

(like a standard VAE decoder), but the term $q_\varphi(\mathbf{t} | \mathbf{z})$ will fail to do so. In situations like this, where the information in \mathbf{t} is *not* subsumed by the information in \mathbf{s} , there is no way for the model to know how to reconstruct a \mathbf{t} . Introducing weight sharing into the bidirectional objective (2) removes this issue, as there is equal opportunity for information from both modalities to enter the latent space, consequently enabling appropriate features to be learned in the decoders $p_\theta(\mathbf{s} | \mathbf{z})$ and $p_\varphi(\mathbf{t} | \mathbf{z})$, which subsequently allow cross generations to be performed.

Furthermore, we also observe that when training with (2) we are able to obtain much more balanced likelihoods Table 2. In this setting we train two models separately using (1) with $\mathbf{s} = \text{MNIST}$ and SVHN and then with $\mathbf{t} = \text{SVHN}$ and $\mathbf{s} = \text{MNIST}$ respectively. At test time, we then ‘flip’ the modalities and the corresponding networks, allowing us to obtain marginal likelihoods in each direction. Clearly we see that we only obtain reasonable marginal likelihoods in the direction for which we train. Training with the bidirectional objective completely removes this deficiency, as we now introduce a balance between the modalities.

Table 2: Marginal likelihoods.

Test Direction	Train Direction		
	$\mathbf{s} = \text{M}, \mathbf{t} = \text{S}$	$\mathbf{s} = \text{S}, \mathbf{t} = \text{M}$	Bi
$\mathbf{s} = \text{M}, \mathbf{t} = \text{S}$	-14733.6	-40249.9 ^{nip}	-14761.3
$\mathbf{s} = \text{S}, \mathbf{t} = \text{M}$	-428728.7 ^{nip}	-11668.1	-11355.4

D Reusing Approximate Posterior MC Sample

When approximating $q_{\varphi,\phi}(\mathbf{t} | \mathbf{s})$ through MC sampling, we find that it is essential for numerical stability to include the sample from the approximate posterior. Before considering why, we must first outline the numerical implementation of $q_{\varphi,\phi}(\mathbf{t} | \mathbf{s})$, which for K samples $\mathbf{z}_{1:K} \sim q_\phi(\mathbf{z} | \mathbf{s})$ is computed using the LogSumExp trick as:

$$\log q_{\varphi,\phi}(\mathbf{t} | \mathbf{s}) \approx \log \sum_{k=1}^K \exp \log q_\varphi(\mathbf{t} | \mathbf{z}_k), \quad (16)$$

where the ratio $\frac{q_\varphi(\mathbf{t} | \mathbf{z})}{q_{\varphi,\phi}(\mathbf{t} | \mathbf{s})}$ is computed as $\exp\{\log q_\varphi(\mathbf{t} | \mathbf{z}) - \log q_{\varphi,\phi}(\mathbf{t} | \mathbf{s})\}$. Given that the LogSumExp trick is defined as:

$$\log \sum_{n=1}^N \exp x_n = x^* + \log \sum_{n=1}^N \exp(x_n - x^*), \quad (17)$$

where $x^* = \max\{x_1, \dots, x_N\}$. The ratio will be computed as

$$\frac{q_\varphi(\mathbf{t} | \mathbf{z})}{q_{\varphi,\phi}(\mathbf{t} | \mathbf{s})} = \exp\{\log q_\varphi(\mathbf{t} | \mathbf{z}) - \log q_\varphi(\mathbf{t} | \mathbf{z}^*) - \log \sum_{k=1}^K \exp[\log q_\varphi(\mathbf{t} | \mathbf{z}_k) - \log q_\varphi(\mathbf{t} | \mathbf{z}^*)]\}, \quad (18)$$

where $\mathbf{z}^* = \arg \max_{\mathbf{z}_{1:K}} \log q_\varphi(\mathbf{t} | \mathbf{z}_k)$. For numerical stability, we require that $\log q_\varphi(\mathbf{t} | \mathbf{z}) \not\gg \log q_\varphi(\mathbf{t} | \mathbf{z}^*)$, otherwise the computation may blow up when taking the exponent. To enforce this, we need to include the sample \mathbf{z} into the LogSumExp function, doing so will cause the first two terms to either cancel if $\mathbf{z} = \mathbf{z}^*$ or yield a negative value, consequently leading to stable computation when taking the exponent.

E Closed Form expression for Wassertein Distance between two Gaussians

. The Wassertein-2 distance between two probability measures μ and ν on \mathbb{R}^n is defined as

$$\mathcal{W}_2(\mu, \nu) := \inf \mathbb{E}(\|X - Y\|_2^2)^{\frac{1}{2}},$$

with $X \sim \mu$ and $Y \sim \nu$. Given $\mu = \mathcal{N}(m_1, \Sigma_1)$ and $\nu = \mathcal{N}(m_2, \Sigma_2)$, the 2-Wassertein is then given as

$$d^2 = \|m_1 + m_2\|_2^2 + \text{Tr}(\Sigma_1 + \Sigma_2 - 2(\Sigma_1^{\frac{1}{2}} \Sigma_2 \Sigma_1^{\frac{1}{2}})^{\frac{1}{2}}).$$

For a detailed proof please see (Givens and Shortt, 2002).

F Additional Results

Table 3: Coherence Scores for MNIST \rightarrow SVHN (Top) and for SVHN \rightarrow MNIST (Bottom). Subscript indicates which modality is always present during training, f indicates the percentage of matched samples. Higher is better.

Model	MNIST \rightarrow SVHN				
	$f = 1.0$	$f = 0.5$	$f = 0.25$	$f = 0.125$	$f = 0.0625$
MEME _{SVHN}	0.625 \pm 0.007	0.551 \pm 0.008	0.323 \pm 0.025	0.172 \pm 0.016	0.143 \pm 0.009
MMVAE _{SVHN}	0.581 \pm 0.008	-	-	-	-
MVAE _{SVHN}	0.123 \pm 0.003	0.110 \pm 0.014	0.112 \pm 0.005	0.105 \pm 0.005	0.105 \pm 0.006
MEME _{MNIST}	0.625 \pm 0.007	0.572 \pm 0.003	0.485 \pm 0.013	0.470 \pm 0.009	0.451 \pm 0.011
MMVAE _{MNIST}	0.581 \pm 0.008	-	-	-	-
MVAE _{MNIST}	0.123 \pm 0.003	0.111 \pm 0.007	0.112 \pm 0.013	0.116 \pm 0.012	0.116 \pm 0.005
MEME _{SPLIT}	0.625 \pm 0.007	0.625 \pm 0.008	0.503 \pm 0.008	0.467 \pm 0.013	0.387 \pm 0.010
MVAE _{SPLIT}	0.123 \pm 0.003	0.108 \pm 0.005	0.101 \pm 0.005	0.101 \pm 0.001	0.101 \pm 0.002

Model	SVHN \rightarrow MNIST				
	$f = 1.0$	$f = 0.5$	$f = 0.25$	$f = 0.125$	$f = 0.0625$
MEME _{SVHN}	0.752 \pm 0.004	0.726 \pm 0.006	0.652 \pm 0.008	0.557 \pm 0.018	0.477 \pm 0.012
MMVAE _{SVHN}	0.735 \pm 0.010	-	-	-	-
MVAE _{SVHN}	0.498 \pm 0.100	0.305 \pm 0.011	0.268 \pm 0.010	0.220 \pm 0.020	0.188 \pm 0.012
MEME _{MNIST}	0.752 \pm 0.004	0.715 \pm 0.003	0.603 \pm 0.018	0.546 \pm 0.012	0.446 \pm 0.008
MMVAE _{MNIST}	0.735 \pm 0.010	-	-	-	-
MVAE _{MNIST}	0.498 \pm 0.100	0.365 \pm 0.014	0.350 \pm 0.008	0.302 \pm 0.015	0.249 \pm 0.014
MEME _{SPLIT}	0.752 \pm 0.004	0.718 \pm 0.002	0.621 \pm 0.007	0.568 \pm 0.014	0.503 \pm 0.001
MVAE _{SPLIT}	0.498 \pm 0.100	0.338 \pm 0.013	0.273 \pm 0.003	0.249 \pm 0.019	0.169 \pm 0.001

F.1 Generative Capability

We report the mutual information between the parameters ω of a pre-trained classifier and the labels y for a corresponding reconstruction \mathbf{x} . The mutual information gives us an indication of the amount of information we would gain about ω for a label y given \mathbf{x} , this provides an indicator to how *out-of-distribution* \mathbf{x} is. If \mathbf{x} is a realistic reconstruction, then there will be a low MI, conversely, an un-realistic \mathbf{x} will manifest as a high MI as there is a large amount of information to be gained about ω . The MI for this setting is given as

$$I(y, \omega | \mathbf{x}, \mathcal{D}) = H[p(y | \mathbf{x}, \mathcal{D})] - \mathbb{E}_{p(\omega | \mathcal{D})} [H[p(y | \mathbf{x}, \omega)]] .$$

Rather than using dropout Gal (2016); Smith and Gal (2018) which requires an ensemble of multiple classifiers, we instead replace the last layer with a sparse variational GP. This allows us to estimate $p(y | \mathbf{x}, \mathcal{D}) = \int p(y | \mathbf{x}, \omega) p(\omega | \mathcal{D}) d\omega$ using Monte Carlo samples and similarly estimate $\mathbb{E}_{p(\omega | \mathcal{D})} [H[p(y | \mathbf{x}, \omega)]]$. We display the MI scores in Table 6, where we see that our model is able to obtain superior results.

G MMVAE baseline with Laplace Posterior and Prior

In Table 7 we display coherence scores using our implementation of MMVAE using a Laplace posterior and prior. Our implementation is inline with the results reported in Shi et al. (2019), indicating that the baseline for MMVAE is accurate.

Table 4: Latent Space Linear Digit Classification.

Model	MNIST				
	1.0	0.5	0.25	0.125	0.0625
MEME _{SVHN}	0.908 ± 0.007	0.881 ± 0.006	0.870 ± 0.007	0.815 ± 0.005	0.795 ± 0.010
MMVAE _{SVHN}	0.886 ± 0.003	-	-	-	-
MVAE _{SVHN}	0.892 ± 0.005	0.895 ± 0.003	0.890 ± 0.003	0.887 ± 0.004	0.880 ± 0.003
Ours _{MNIST}	0.908 ± 0.007	0.882 ± 0.003	0.844 ± 0.003	0.824 ± 0.006	0.807 ± 0.005
MMVAE _{MNIST}	0.886 ± 0.003	-	-	-	-
MVAE _{MNIST}	0.892 ± 0.005	0.895 ± 0.002	0.898 ± 0.004	0.896 ± 0.002	0.895 ± 0.002
MEME _{SPLIT}	0.908 ± 0.007	0.914 ± 0.003	0.893 ± 0.005	0.883 ± 0.006	0.856 ± 0.003
MVAE _{SPLIT}	0.892 ± 0.005	0.898 ± 0.005	0.895 ± 0.001	0.894 ± 0.001	0.898 ± 0.001

Model	SVHN				
	1.0	0.5	0.25	0.125	0.0625
MEME _{SVHN}	0.648 ± 0.012	0.549 ± 0.008	0.295 ± 0.025	0.149 ± 0.006	0.113 ± 0.003
MMVAE _{SVHN}	0.499 ± 0.045	-	-	-	-
MVAE _{SVHN}	0.131 ± 0.010	0.106 ± 0.008	0.107 ± 0.003	0.105 ± 0.005	0.102 ± 0.001
Ours _{MNIST}	0.648 ± 0.012	0.581 ± 0.008	0.398 ± 0.029	0.384 ± 0.017	0.362 ± 0.018
MMVAE _{MNIST}	0.499 ± 0.045	-	-	-	-
MVAE _{MNIST}	0.131 ± 0.010	0.106 ± 0.005	0.106 ± 0.003	0.107 ± 0.005	0.101 ± 0.005
MEME _{SPLIT}	0.648 ± 0.012	0.675 ± 0.004	0.507 ± 0.003	0.432 ± 0.011	0.316 ± 0.020
MVAE _{SPLIT}	0.131 ± 0.010	0.107 ± 0.003	0.109 ± 0.003	0.104 ± 0.007	0.100 ± 0.008

Table 5: Correlation Values for CUB cross generations. Higher is better.

Model	Image → Captions				
	GT	$f = 1.0$	$f = 0.5$	$f = 0.25$	$f = 0.125$
MEME _{Image}	0.106 ± 0.000	0.064 ± 0.011	0.042 ± 0.005	0.026 ± 0.002	0.029 ± 0.003
MMVAE _{Image}	0.106 ± 0.000	0.060 ± 0.010	-	-	-
MVAE _{Image}	0.106 ± 0.000	-0.002 ± 0.001	-0.000 ± 0.004	0.001 ± 0.004	-0.001 ± 0.005
MEME _{Captions}	0.106 ± 0.000	0.064 ± 0.011	0.062 ± 0.006	0.048 ± 0.004	0.052 ± 0.002
MMVAE _{Captions}	0.106 ± 0.000	0.060 ± 0.010	-	-	-
MVAE _{Captions}	0.106 ± 0.000	-0.002 ± 0.001	-0.000 ± 0.004	0.000 ± 0.003	0.001 ± 0.002
MEME _{SPLIT}	0.106 ± 0.000	0.064 ± 0.011	0.046 ± 0.005	0.031 ± 0.006	0.027 ± 0.005
MVAE _{SPLIT}	0.106 ± 0.000	-0.002 ± 0.001	0.000 ± 0.003	0.000 ± 0.005	-0.001 ± 0.003

Model	Caption → Image				
	GT	$f = 1.0$	$f = 0.5$	$f = 0.25$	$f = 0.125$
MEME _{Image}	0.106 ± 0.000	0.074 ± 0.001	0.058 ± 0.002	0.051 ± 0.001	0.046 ± 0.004
MMVAE _{Image}	0.106 ± 0.000	0.058 ± 0.001	-	-	-
MVAE _{Image}	0.106 ± 0.000	-0.002 ± 0.001	-0.002 ± 0.000	-0.002 ± 0.001	-0.001 ± 0.001
Ours _{Captions}	0.106 ± 0.000	0.074 ± 0.001	0.059 ± 0.003	0.050 ± 0.001	0.053 ± 0.001
MMVAE _{Captions}	0.106 ± 0.000	0.058 ± 0.001	-	-	-
MVAE _{Captions}	0.106 ± 0.000	0.002 ± 0.001	-0.001 ± 0.002	-0.003 ± 0.002	-0.002 ± 0.001
MEME _{SPLIT}	0.106 ± 0.000	0.074 ± 0.001	0.061 ± 0.002	0.047 ± 0.003	0.049 ± 0.003
MVAE _{SPLIT}	0.106 ± 0.000	-0.002 ± 0.001	-0.002 ± 0.002	-0.002 ± 0.001	-0.002 ± 0.001

Table 6: Mutual Information Scores. Lower is better.

Model	MNIST				
	1.0	0.5	0.25	0.125	0.0625
Ours _{SVHN}	0.075 ± 0.002	0.086 ± 0.003	0.101 ± 0.002	0.102 ± 0.004	0.103 ± 0.001
MMVAE _{SVHN}	0.105 ± 0.004	-	-	-	-
MVAE _{SVHN}	0.11 ± 0.00551	0.107 ± 0.007	0.106 ± 0.004	0.106 ± 0.012	0.142 ± 0.007
Ours _{MNIST}	0.073 ± 0.002	0.087 ± 0.001	0.101 ± 0.001	0.099 ± 0.001	0.104 ± 0.002
MMVAE _{MNIST}	0.105 ± 0.004	-	-	-	-
MVAE _{MNIST}	0.11 ± 0.00551	0.102 ± 0.00529	0.1 ± 0.00321	0.1 ± 0.0117	0.0927 ± 0.00709
Model	SVHN				
	1.0	0.5	0.25	0.125	0.0625
Ours _{SVHN}	0.036 ± 0.001	0.047 ± 0.002	0.071 ± 0.003	0.107 ± 0.007	0.134 ± 0.003
MMVAE _{SVHN}	0.042 ± 0.001	-	-	-	-
MVAE _{SVHN}	0.163 ± 0.003	0.166 ± 0.010	0.165 ± 0.003	0.164 ± 0.004	0.176 ± 0.004
Ours _{MNIST}	0.036 ± 0.001	0.048 ± 0.001	0.085 ± 0.006	0.111 ± 0.004	0.142 ± 0.005
MMVAE _{MNIST}	0.042 ± 0.001	-	-	-	-
MVAE _{MNIST}	0.163 ± 0.003	0.175 ± 0.00551	0.17 ± 0.0102	0.174 ± 0.012	0.182 ± 0.00404

Table 7: Coherence Scores for MMVAE using Laplace posterior and prior.

MNIST	SVHN
91.8%	65.2%